International Journal of Fatigue 170 (2023) 107505

Contents lists available at ScienceDirect

International Journal of Fatigue

journal homepage: www.elsevier.com/locate/ijfatigue

Effect of crack flank holes on fatigue crack growth

D.M. Neto [a,*], N. Cavaleiro [a], E.R. Sérgio [a], J. Jesus [a,b], A. Camacho-Reyes [c], F.V. Antunes [a]

[a] CEMMPRE, Centre for Mechanical Engineering, Materials and Processes, University of Coimbra, Mechanical Engineering Department, Pinhal de Marrocos, 3030-788 Coimbra, Portugal
[b] Department of Mechanical Engineering, Lisbon Polytechnic – ISEL, Rua Conselheiro Emídio Navarro 1, 1959-007 Lisboa, Portugal
[c] Departamento de Ingeniería Mecánica y Minera, University of Jaén, Jaén, Spain

ARTICLE INFO

Keywords:
Fatigue crack growth
CT specimen
Crack flank holes
Crack closure
Numerical simulation

ABSTRACT

The effect of drilling two symmetric holes along the crack flanks on the fatigue crack growth (FCG) rate was evaluated numerically. The FCG increases (decreases) when the crack tip is behind (ahead) the holes. This behaviour is enlarged both by increasing the diameter of the holes and by reducing the distance between them. This is consequence of the geometrical effect, which modifies the plastic zone size. Experimental work validated the numerical model, indicating that that cumulative plastic strain at the crack tip is an adequate crack driving force and that cyclic plastic deformation is the main damage mechanism of FCG.

1. Introduction

Fatigue crack growth (FCG) depends on environment, loading, material and geometry. Crack closure phenomenon has been able to explain the effect of different loading parameters, particularly under plane stress conditions. According to this concept, there is an opening load below which there is no fatigue damage, therefore the effective load range is $K_{max}-K_{open}$, being K_{max} and K_{open} the maximum and opening stress intensity factors (SIF), respectively [1]. In fact, crack closure phenomenon was used to explain the effect of different loading parameters, namely, stress ratio [2], K_{max} [3], overloads [3,4] and Superblock 2020 load pattern [5]. Crack closure was also able to explain the effect of residual stresses on FCG [6]. The presence of tensile stresses ahead of the crack tip increases the FCG rate, while compressive stresses reduce it. Nevertheless, this effect disappears when the contact of the crack flanks is eliminated. Finally, crack closure was also able to explain the effect of some geometrical parameters, namely the specimen's thickness and the presence of notches. In fact, the effect of thickness is usually associated with crack closure phenomenon. The increase of the thickness yields an increase of *da/dN* [7], due to the reduction of the influence of near-surface regions, where crack closure is more relevant. Borges *et al.* [8] studied FCG from circular notches. Under plane stress conditions the contact of crack flanks reduces substantially the effect of notch radius and the size of the notch affected zone. On the other hand, the difference between *da/dN* values for CT (compact tension) and MT (middle tension) specimen geometries is usually attributed to *T*-stress effects. Tong et al. [9] showed that the fatigue crack growth of a crack in a CT sample is up to ten times higher than that measured in single edge notched tension (SENT) or centre crack tension (CCT) samples, with the same thickness. The authors argued that this difference is due to the *T*-stress, positive in CT samples and negative in CCT and SENT samples. It would be interesting to study the relevance of crack closure for other geometrical details, namely in the presence of lateral holes.

Ayatolahi et al. [10] proposed the use of symmetrical lateral holes to arrest a crack. They studied SENT specimens with width W = 50 mm, made of 2024-T3 aluminium alloy. The finite element method was used to calculate the stress intensity factors and NASGRO equation was used to predict *da/dN*. When the crack extends towards the flank holes, the SIF initially increases and then decreases. It reaches its minimum value almost at the end of the region between flank holes, with a reduction of 41 % with respect to the plain model. Reducing the distance between holes decreased the crack tip stress and enhanced the improving effects. Moreover, larger hole diameters resulted in more reduction in the stress intensity factor. Shin et al. [11] suggested that the best retardation effect could be achieved when the hole was very near to the crack plane and slightly ahead of the crack tip. Chen et al. [12] studied the effect of circular crack flank holes on maximum plastic strain range and the ratchet limit. They reported that the optimum location of holes, where the most reduction of maximum plastic strain range occurred with minimum effect on the ratchet limit, was located at a distance equal to 10 % of semi-crack length, behind the crack tip; in addition, this location was independent of the holes diameter. However, the typical solution to

* Corresponding author.
E-mail address: diogo.neto@dem.uc.pt (D.M. Neto).

https://doi.org/10.1016/j.ijfatigue.2023.107505
Received 14 October 2022; Received in revised form 29 December 2022; Accepted 4 January 2023
Available online 7 January 2023

arrest cracks is drilling a single hole at the crack tip, which turns the sharp crack into a round-tip notch. This technique is widely employed for cracks detected in the aircraft skin and in steel bridges [13–15]. Song et al. [16] studied the effect of stop-hole diameter and reported that larger diameters resulted in longer fatigue lives. The introduction of compressive residual stress around the stop-hole edge using cold expansion improves fatigue life [17]. The insertion of pins into the stop holes is also beneficial [18]. Razavi et al. [19] studied the effect of two kinds of stop-hole drilling on the fatigue life extension, under mixed mode loading conditions. The hole drilling technique compete with other techniques to extend the fatigue life of cracked structures that cannot be replaced as soon as the crack is detected, namely crack filling [20,21], application of patches [22], and introduction of compressive residual stresses. The residual compressive stresses can be generated by use of overloading [23], indentation [24,25], laser shock peening [26,27], shot peening [28] and spot heating [29].

The objective of this research it to study the effect of lateral holes on FCG, checking the effectiveness of its capabilities to arrest the crack. The fundamental mechanisms are identified, and the relevance of crack closure is quantified. A numerical approach was used to predict FCG rate, based on cumulative plastic strain at the crack tip [30]. The numerical approach assumes that cyclic plastic deformation is the main damage mechanism responsible for fatigue crack growth. Although the plastic zone size is effectively much smaller than the elastic region, the crack tip is always surrounded by a plastic zone, defining the irreversible phenomenon of fatigue crack growth. Thus, the crack tip node is released when this cumulative strain reaches a critical value, which is supposed to be a material property. This approach includes the effects of plasticity induced crack closure, residual stresses, partial closure, crack tip blunting and material hardening. The load range below crack opening, contrarily to what is stated by crack closure concept, has an effect on crack tip damage [3], which is also included in the model. The prediction capabilities of this approach were proved with direct comparisons between experimental results and numerical predictions, particularly under variable amplitude conditions. In fact, Borges *et al.* [31] successfully predicted the effect of ΔK observed experimentally in 2024-T251 aluminium alloy and 18Ni300 steel, Neto *et al.* [32] predicted the effect of stress ratio, Neto *et al.* [5] predicted the effect of Superblock2020 load pattern and Neto et al. [33] predicted the effect of load blocks in AA6082-T6. Anyway, an additional validation was made here by comparing experimental results, obtained in CT specimens with lateral holes made of 2050-T8 aluminium alloy, with numerical predictions.

2. Numerical model

The numerical simulations were performed with the in-house finite element code DD3IMP, which was originally developed for the numerical simulation of sheet metal forming processes [34]. In order to numerically study the effect of the holes near the crack tip, a pair of holes was introduced in a CT specimen. Fig. 1 presents the geometry of the CT specimen, where D is the drilled hole's diameter and V is the vertical position in respect to the specimen's symmetry plane. In addition to the classical CT specimen without any hole, four different CT specimen with a pair of holes were created, using the dimension and position of the holes listed in Table 1. Three diameters were considered along with two vertical distances. The most important parameter is the relative position of the holes relative to the crack tip. Nevertheless, the initial crack length dictates the size of the plastic zone around the crack tip, which is affected by the presence of the drilled holes. Thus, the effect of crack flank holes on fatigue crack growth is more significant for large values of crack length since the plastic zone expands to the region surrounding the holes. Note that the lateral holes were drilled 1 mm ahead of the initial crack tip position.

Due to the symmetry in terms of loading and geometry, it was possible to consider only 1/4 of the specimen, using adequate boundary

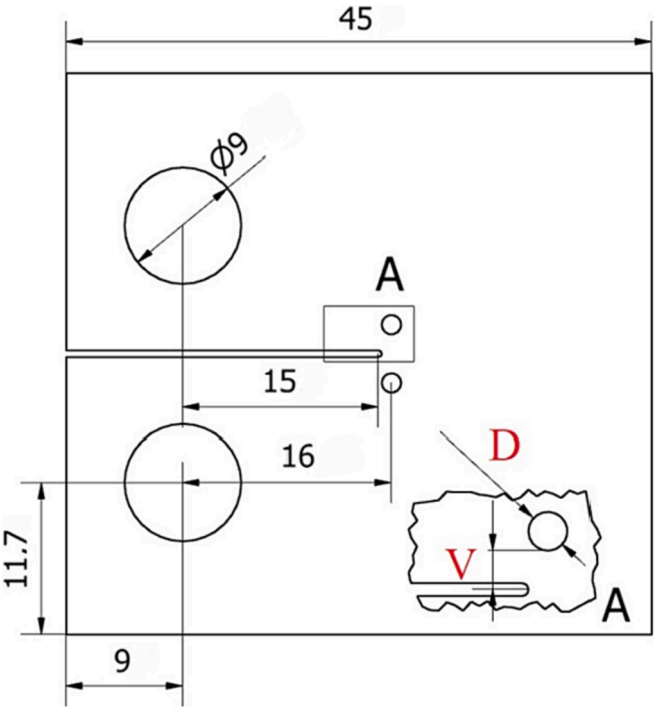

Fig. 1. CT specimen geometry with a pair of holes near the crack tip, which position is defined by its diameter (D) and vertical position in relation to the symmetry axis (V).

Table 1
CT specimen dimensions and location of the drilled holes.

Characteristic Dimension, W [mm]	Initial crack length, a_0 [mm]	D [mm]	V [mm]
36	15	Without holes	
		0.5	1
		1	1
		1.5	1
		1.5	1.5

conditions. The thickness assumed for all CT specimens was 0.1 mm. All specimen geometries were loaded assuming both plane strain and plane stress states. This change can be easily carried out in the numerical model by updating the boundary conditions, allowing to assess the effect of crack flank holes on fatigue crack growth, considering both thin and tick plates. For this study, the load is characterized by constant amplitude, ranging from $F_{min} = 3.5$N to $F_{max} = 35$N ($R = 0.1$), which are small values due to the thickness value adopted.

The numerical simulation of FCG is based on the cumulative plastic strain at the crack tip. Therefore, the elastic–plastic behaviour of the material must be accurately modelled. The material used in this study is the 2024-T351 aluminium alloy. The elastic behaviour was defined by the Hooke's law, using the Young modulus (E) and Poisson ratio (ν), both listed in Table 2. The plastic behaviour was described with the von Mises yield criterion coupled with a mixed hardening model using the Swift isotropic and Lemaitre-Chaboche kinematic hardening laws, under

Table 2
Mechanical properties for the 2024-T351 aluminium alloy. Adapted from [31].

Young Modulus [GPa]	Poisson's Coefficient	Swift law			Lemaitre-Chaboche model	
		Y_0 [MPa]	K [MPa]	n	X_{Sat} [MPa]	C_X
72.26	0.29	288.96	389	0.056	111.84	138.80

an associated flow rule. The Swift isotropic hardening law [35] is given by:

$$Y = K\left((Y_0/K)^{1/n} + \bar{\varepsilon}^{p}\right)^{n} \quad (1)$$

where Y is the flow stress and $\bar{\varepsilon}^{p}$ denotes the equivalent plastic strain. The material parameters of Swift law are K, Y_0 and n. The Lemaitre-Chaboche law describes the non-linear kinematic hardening as follows [36]:

$$\dot{\mathbf{X}} = C_X\left[X_{Sat}\frac{\boldsymbol{\sigma}^{'} - \boldsymbol{X}}{\bar{\sigma}} - \boldsymbol{X}\right]\dot{\bar{\varepsilon}}^{p} \quad (2)$$

where $\boldsymbol{X}$ is the back-stress tensor, $\bar{\sigma}$ is the equivalent stress, $\boldsymbol{\sigma}^{'}$ is the deviatoric Cauchy stress tensor, $\dot{\bar{\varepsilon}}^{p}$ is the equivalent plastic strain rate and C_X and X_{Sat} are material parameters, which denote the saturation rate and the norm of the saturated back-stress tensor, respectively. The calibration of the material parameters was performed by minimising the difference between the numerical and the experimental results of stress–strain curves obtained in low cycle fatigue tests. The obtained set of material parameters is presented in Table 2 [31].

The model of each specimen was discretized with linear hexahedral finite elements, using a single layer of elements in the thickness direction. In order to reduce the computational cost of the numerical simulations, each mesh is composed by two regions, a regular fine mesh around the crack tip with 8 μm of mesh size and an unstructured coarse mesh far away from the crack tip. The plastic deformation generated around the crack tip occurs always within the region of the fine mesh. Fig. 2 presents the finite element mesh of the CT specimen considering a hole with $D = 1.5$ mm and $V = 1.0$ mm. This mesh is composed by 14,353 finite elements and 29,868 nodes. Note that every mesh has the same configuration, only changing the number of elements near the drilled hole in order to achieve a smooth transition between element sizes in the different zones. The initial crack length was defined using adequate boundary conditions at the nodes located in the horizontal symmetry plane (see Fig. 2), i.e. the notch was neglected in the numerical model.

The crack propagation was carried out by node release along the symmetry plane. The crack increment is dictated by the mesh size along the crack path, which corresponds to 8 μm in the adopted meshes. The node release occurs when the cumulative plastic strain at the crack tip, ε_p, reaches a critical value, ε_p^c. Thus, the FCG rate is calculated by the ratio between the mesh size and the number of load cycles required to achieve the critical value of plastic strain. Note that the calibration procedure used to obtain the critical value of plastic strain must be carried out using same mesh size used in the FCG analysis, allowing to obtain a negligible effect of the mesh size on the predicted FCG rate. The plastic strain value at the crack tip results from the average between the two values, obtained at the integration points (Gauss points) immediately behind and ahead of the crack tip. Fig. 3 shows an example of the evolution of plastic strain at the crack tip throughout 100 load cycles. Each drop in the plastic strain corresponds to a nodal release, i.e. the

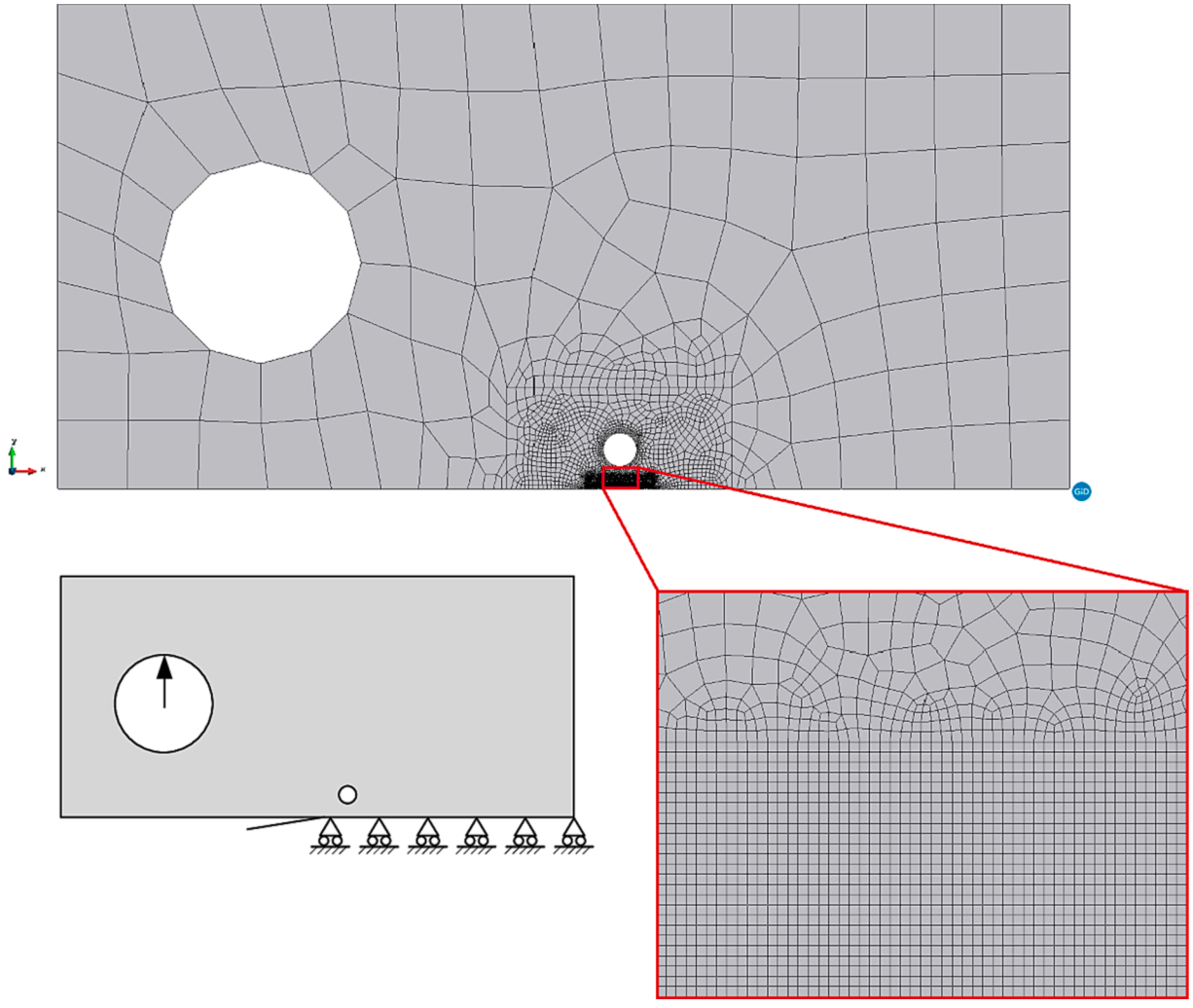

Fig. 2. Finite element mesh of the CT specimen considering a pair of holes ($D = 1.5$ mm; $V = 1.0$ mm) near the crack tip.

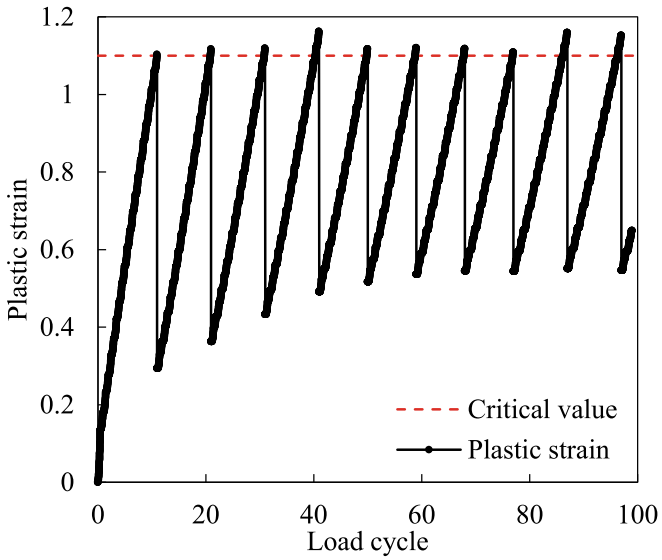

Fig. 3. Evolution of plastic strain at the crack tip during the first 10 propagations, for the CT specimen considering a pair of holes with $D = 1.5$ mm and $V = 1.0$ mm, under plane stress state.

crack tip node is moved to the following node. The plastic strain at the crack tip progressively increases between each node release until achieving the predefined critical value. Besides, the plastic strain after the node release is not zero because it is assumed that damage accumulation occurs during the entire cyclic loading, even when the element is not immediately ahead of the crack tip. The value of plastic strain after each node release is increasing until reaches a steady state regime, indicating that the plastic zone size is increasing ahead the crack tip, which is significative larger than the element size. In some cases, propagation occurs for slightly higher values of plastic strain because the node release only occurs at the minimum load instant.

In order to determine the critical value of plastic strain involved in the node release approach, a calibration procedure is required. Hence, a single experimental value of *da/dN* obtained under constant amplitude loading for a specific crack length and stress ratio is compared with *da/dN* predicted numerically, using different values of critical plastic strain. Typically, this procedure is carried out in the Paris regime for a relatively large stress intensity factor, where the environment effect (more aggressive in low load ranges) is less relevant. The fitting between numerical and experimental *da/dN* was obtained for this aluminium alloy using a critical plastic strain of 110 %. This value, which is supposed to be a material property, was obtained in a previous work of the authors for this aluminium alloy [31].

3. Numerical results

Fig. 4 shows the effect of the pair of small holes drilled near the crack tip on the FCG rate, assuming both plane stress and plane strain states. The dashed vertical lines represent the left and right limits of the holes ($D = 1.0$ mm and $V = 1.0$ mm). The results show that the holes induce an increase of the FCG rate when the crack tip is located behind the centre of the holes ($a < 16$ mm). On the other hand, when the crack tip is located ahead the centre of the holes ($a > 16$ mm), the presence of the holes leads to a decrease of the FCG rate in comparison to the values obtained for specimen without holes. Thus, *da/dN* curves intersect for a crack length $a = 15.8$ mm, i.e., when the crack tip is close to the centre of the holes. Note that the severe decrease of *da/dN* at the beginning of each numerical simulation is due to the formation of the plastic wake, where the crack closure level is increasing until it reaches a steady state regime. This behaviour is larger under plane stress state. Nevertheless, the global effect of the small holes on the predicted FCG rate is identical under both plane stress and plane strain states, as shown in Fig. 4. Despite the effect of the holes on the FCG disappears when the crack tip is farther from the holes, the numerical simulations were performed considering an initial crack length only 1 mm behind the centre of the hole.

The position of the small holes in relation to the crack tip position affects the stress field around the crack tip. Hence, the stress distribution around the crack tip was evaluated under plane stress conditions for a static load of 35 N. Fig. 5 presents both the stress field predicted in the specimen with small holes ($D = 1.0$ mm and $V = 1.0$ mm) and the predicted in the specimen without small holes. Two different values of crack length ($a = 15.25$ mm and $a = 16.75$ mm) were considered, i.e. the crack tip located behind the small holes and the crack tip located ahead the small holes. Considering the specimen without small holes, the increase of the crack length leads to an increase in the plastic zone size around the crack tip due to the increase of the stress intensity factor value. The plastic zone, i.e. the region around the crack tip where the material points experienced a von Mises stress larger than the yield stress, is indicated by white colour surrounding the maximum elastic stress value. For the crack length of $a = 15.25$ mm, the plastic zone size increases when the small holes are introduced in the specimen (see Fig. 5 (a) and Fig. 5 (c)). On the other hand, for the crack length of $a = 15.75$ mm, the inclusion of the small holes leads to a slight decrease of the plastic zone size (see Fig. 5 (b) and Fig. 5 (d)). Therefore, the effect of the

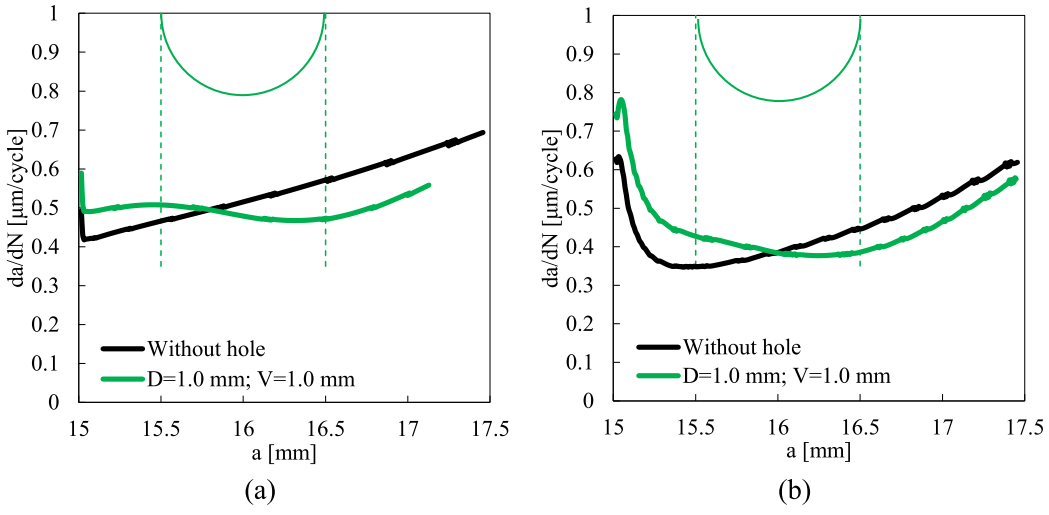

Fig. 4. Effect of the small holes presence on the predicted FCG rate: (a) plane strain state; (b) plane stress state.

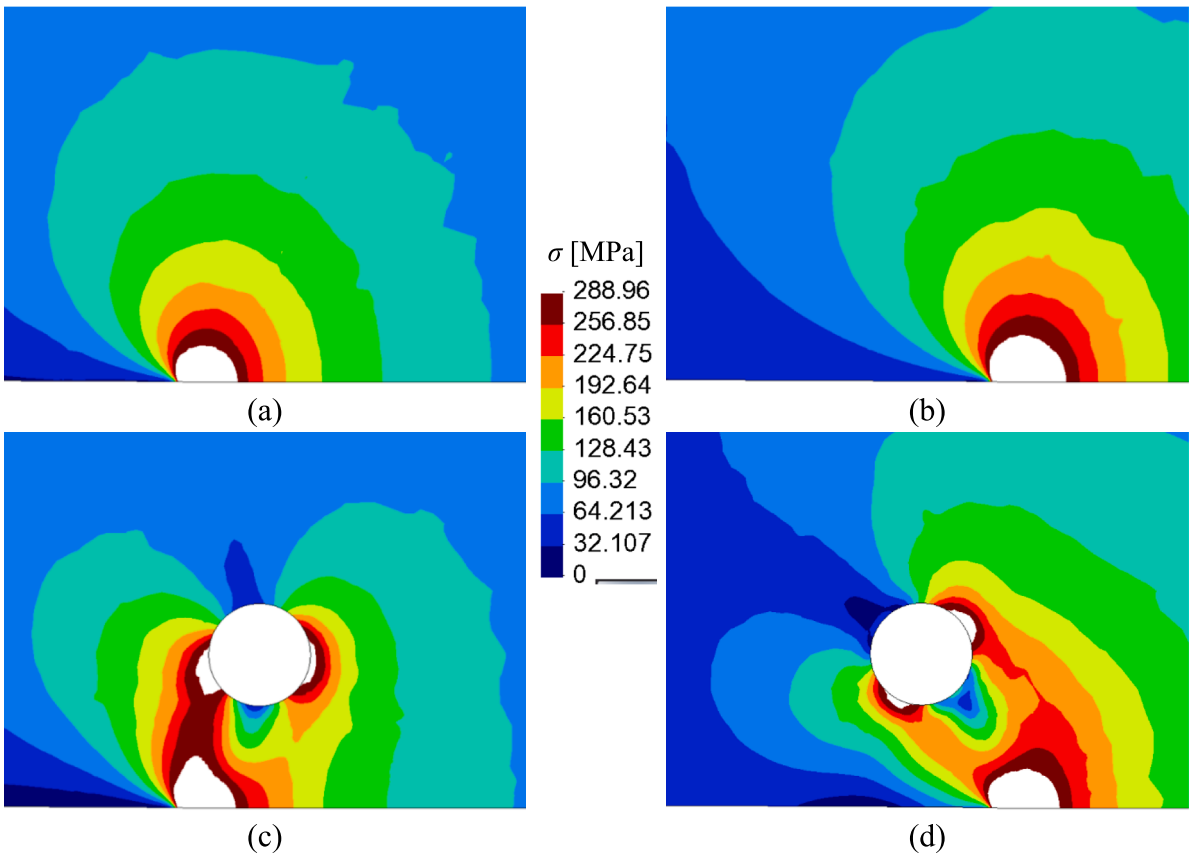

Fig. 5. Predicted equivalent stress distribution around the crack tip for a static load of 35 N under plane stress conditions: (a) without small holes for $a = 15.25$ mm; (b) without small holes for $a = 16.75$ mm; (c) with small holes for $a = 15.25$ mm; (d) with small holes for $a = 16.75$ mm. Plastic zone near the crack tip represented by white colour.

small holes on the FCG rate observed in Fig. 4 is due to the change of the stress field near the crack tip and, consequently, plastic zone size.

The plastic zone is always enlarging along the crack propagation direction due to the inherent movement of the crack tip. Fig. 6 presents the total plastic zone predicted in the specimen with small holes ($D = 1.0$ mm and $V = 1.0$ mm), after 2 mm of crack propagation, which is compared with the plastic zone predicted in the specimen without small holes. In the absence of holes, the plastic zone size around the crack tip is slightly increasing with the crack length increase (see Fig. 6 (a)-(b)), which agrees with the evolution of the stress intensity factor value. Besides, the numerical simulation under plane stress leads to a global enlargement of the plastic zone, in comparison with the numerical prediction obtained under plane strain. In the case of the specimens with small holes, although the highest levels of plastic strain occur along the crack path direction, the plastic zone extends to the hole location, particularly under plane stress (see Fig. 6 (d)). In fact, the inclusion of the holes does not change the size of the plastic zone along the crack direction. Nevertheless, the size of the plastic zone perpendicular to the crack flanks is influenced by the drilled holes, as shown in the predicted equivalent stress distribution around the crack tip (see Fig. 5). When the crack tip is located behind the small holes, an enlargement of the plastic zone is observed in comparison with the situation without holes. On the other hand, when the crack tip is located immediately ahead the small holes, the plastic zone is slightly reduced in comparison with the situation without holes. Under the plane stress condition, the predicted size of the plastic zone was evaluated perpendicularly to the crack flanks for $a = 16.5$ mm, obtaining 0.7 mm for the specimen with holes and 0.9 mm for the specimen without holes (see Fig. 6). This behaviour is a consequence of the redistribution of the stress field around the crack tip, due to the presence of the holes. Therefore, the effect of the small holes on the plastic zone size agrees with the FCG rate evolution shown in Fig. 4.

3.1. *Effect of the diameter of the holes*

Fig. 7 presents the effect of the hole diameter (for the same vertical position) on FCG rate, comparing plane strain and plane stress states. The dashed vertical lines represent the left and right limits of each hole. In both situations, the effect of holes diameter on fatigue crack growth is noticeable, increasing for larger diameters. Comparing with the FCG rate evaluated in the specimen without holes, the presence of the small holes leads to an increase of the FCG rate for $a < 16$ mm and decrease of the FCG rate for $a > 16$ mm. In addition to the complexity associated to the operation of drilling holes near the crack tip, the inclusion of the holes is only beneficial when they are located behind the crack tip. This behaviour of the FCG rate agrees with the results of plastic zone size presented in Fig. 6. Under plane strain conditions, the effect of the small holes on the FCG rate seams stronger when the crack is ahead of the holes, while under plane stress conditions the higher effect is observed when the crack is behind the holes. Note that, for plane stress state, the plastic wake is under formation during the crack propagation, until a crack length of 15.5 mm, leading to a decrease in the evolution of the FCG rate. The intersection with *da/dN* curve without hole is not affected by hole's diameter under plane strain state but moves towards larger crack lengths under plane stress conditions. When the crack tip is far away from the centre of the hole, the hole effect must vanish, i.e. the FCG rate converges to the one obtained using the specimen without holes.

Since the initial crack length ($a_0 = 15$ mm) used in the numerical simulation is relatively close to the holes position, the FCG rate is influenced from the beginning, not allowing the evaluation of the crack

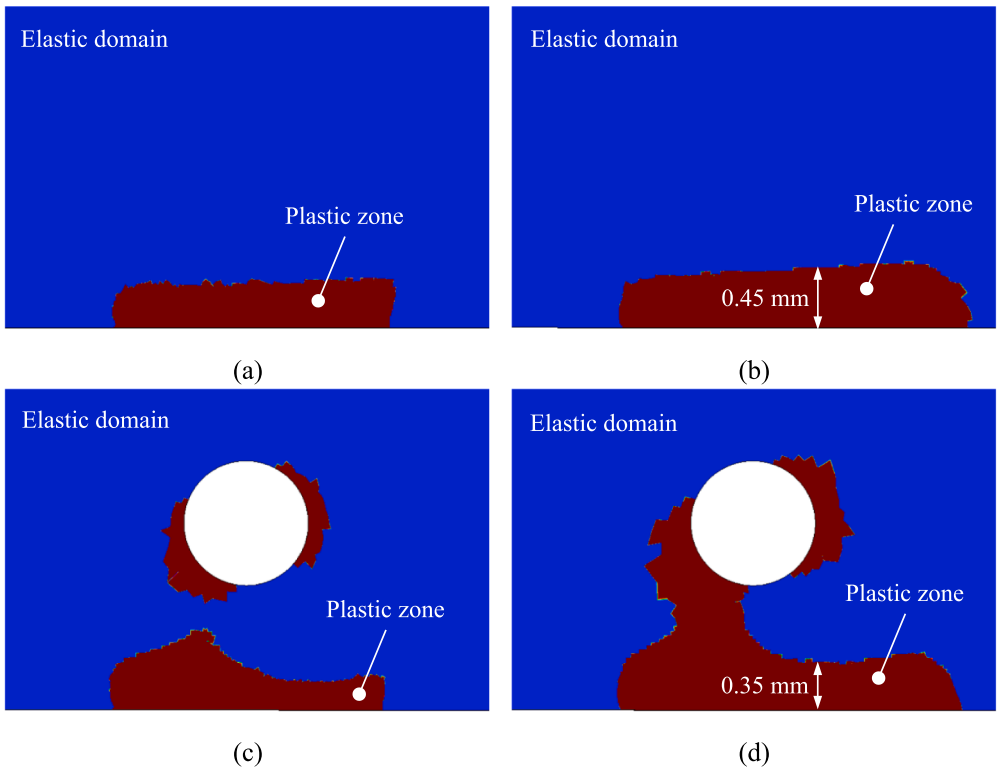

Fig. 6. Predicted plastic zone after 2 mm of propagation ($a = 17$ mm): (a) without small holes under plane strain; (b) without small holes under plane stress; (c) with small holes under plane strain; (d) with small holes under plane stress.

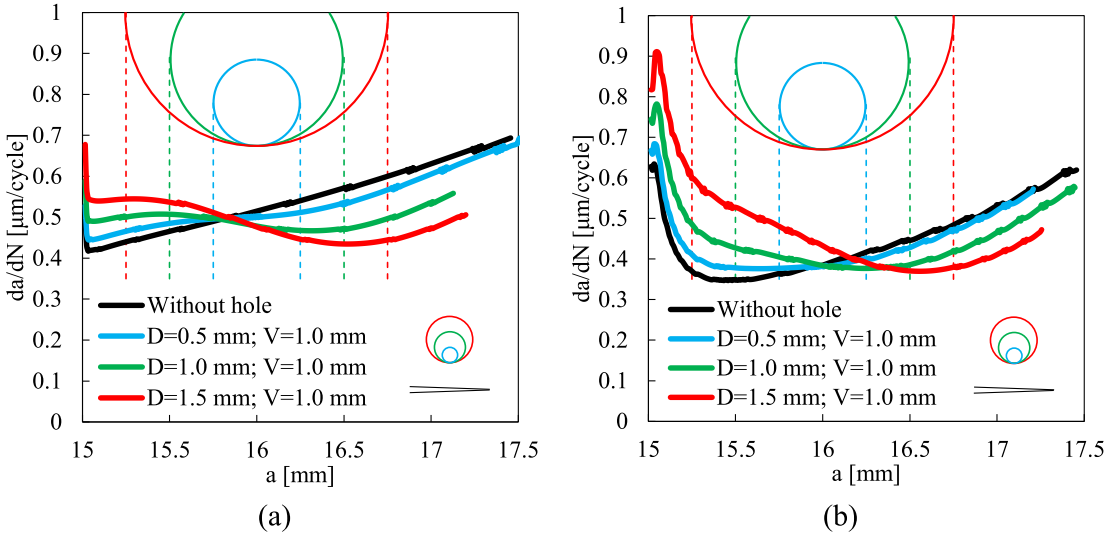

Fig. 7. Effect of the hole diameter (D) on the FCG rate for the same vertical position ($V = 1$ mm): (a) plane strain state; (b) plane stress state.

extension affected by the holes. Thus, Fig. 8 presents the effect of the hole diameter on the number of load cycles required for each 0.5 mm of crack length increment, considering the range of crack length from 15 mm to 17 mm.

Since the FCG rate evolution is continuously increasing in the specimen without holes, except at the very beginning of the simulation using plane stress conditions (see Fig. 7 (b)), the number of load cycles required to propagate 0.5 mm is constantly decreasing. Considering this range of crack length (15–17 mm), which is near the drilled holes, the opposite behaviour was observed for the specimens with holes, particularly for the larger value of diameter ($D = 1.5$ mm). This indicates a local decrease of the FCG rate near the holes. Using plane strain conditions, the total number of load cycles, required to propagate the crack until a length of 17 mm, was lower in the specimen without holes (see Table 3). Thus, the inclusion of the holes is beneficial for this range of crack length. Nevertheless, adopting plane stress conditions in the simulation, the total number of load cycles required to propagate the crack until 17 mm of length was higher in the specimen without holes (see Table 3), indicating that the inclusion of the holes is not beneficial in increasing the fatigue life. This opposite conclusion between plane strain and plane stress is a consequence of two factors: (i) analysis for a small portion of propagation length (2 mm) and (ii) higher effect of the holes under plane strain and plane stress conditions occurs for the crack tip ahead (FCG rate reduction) and behind (FCG rate increase),

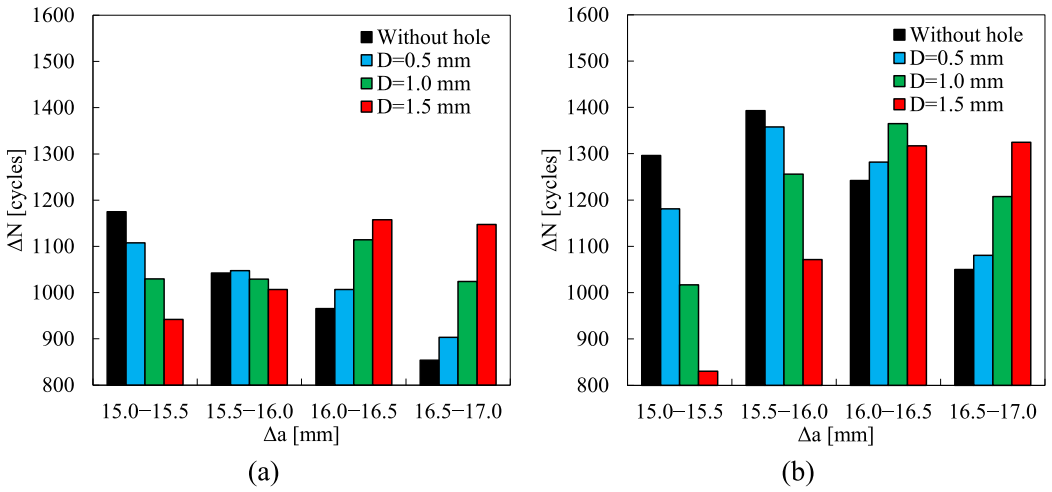

Fig. 8. Effect of the hole diameter (D) on the number of load cycles required to achieve 0.5 mm of crack length increment for the same vertical position ($V = 1$ mm): (a) plane strain state; (b) plane stress state.

Table 3
Predicted total number of load cycles required to propagate from 15 mm to 17 mm for different values of hole diameter (D) and $V = 1$ mm.

	Without hole	$D = 0.5$ mm	$D = 1.0$ mm	$D = 1.5$ mm
Plane strain	4037	4065	4197	4254
Plane stress	4981	4902	4845	4544

respectively. Globally, the inclusion of the holes is beneficial only when the crack tip is ahead the holes (a > 16 mm) but that gain in load cycles can be quickly reverted by the detrimental effect when the crack tip is located behind the holes. So, if the holes are drilled to improve fatigue life, they must be centred with the crack tip. In fact, the only way to avoid the increase of the fatigue crack growth rate caused by the holes is to perform the drilling of the holes behind the crack tip. A better alternative is to drill a hole along the crack front, in order to eliminate the crack singularity.

3.2. Effect of the vertical position of the holes

Fig. 9 presents the effect of the distance between the two drilled holes on the FCG rate. Accordingly, two different vertical positions were considered for the same hole diameter ($D = 1.5$ mm) and compared with the situation without small holes in the vicinity of the crack. When the holes are located behind the crack tip, the effect of the holes is stronger under plane strain conditions. On the other hand, when the holes are located ahead of the crack tip, the effect of the holes is stronger under the plane stress state. In both cases, the effect of the holes is stronger when they are located closer to the crack. Increasing the vertical position of the small hole with respect to the specimen's symmetry plane from $V = 1$ mm to $V = 1.5$ mm leads to a significant loss of the hole's effect on the FCG rate, particularly when the holes are located behind the crack tip and under plane stress conditions. Indeed, the effect of the holes must disappear when they are located far away from the crack, i.e. the FCG rate will converge to values corresponding to the specimen without holes when the crack tip is moving away from the location of the holes.

3.3. Effect of the contact between crack flanks

The numerical modelling of crack closure requires the occurrence of physical contact between the crack flanks during the unloading stage.

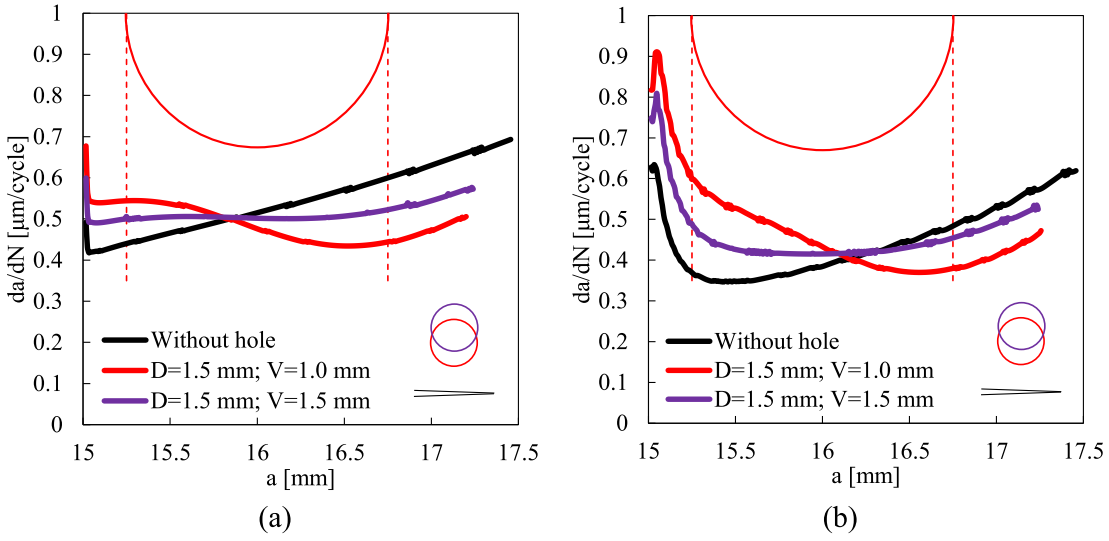

Fig. 9. Effect of the vertical position of the holes relatively to the symmetry plane (V) on the FCG rate for the same diameter ($D = 1.5$ mm): (a) plane strain state; (b) plane stress state.

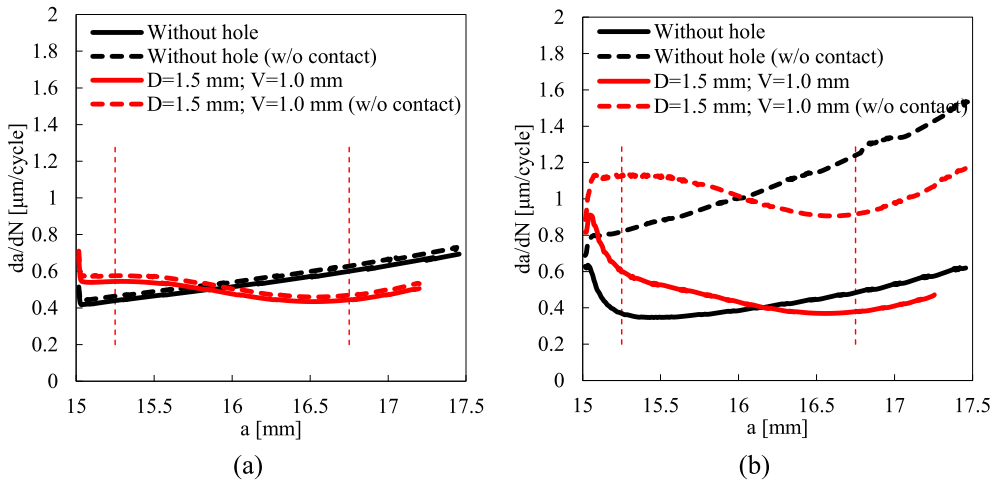

Fig. 10. Effect of neglecting the contact of the crack flanks on FCG rate for the situation without holes and for $D = 1.5$ mm; $V = 1.0$ mm: (a) plane strain state; (b) plane stress state.

Fig. 10 presents the effect of this contact, between the crack flanks, on the FCG rate evolution, considering both the specimen with holes ($D = 1.5$ mm and $V = 1$ mm) and the specimen without holes. The contact between the crack flanks was disabled numerically, analysing both plane strain and plane stress conditions. Under plane strain, the contact between crack flanks has no significant effect on the FCG rate, as shown in Fig. 10 (a). For both specimens studied, there is only a slight increase of the FCG rate, which indicates that under plane strain state there is almost no crack closure.

On the other hand, under plane stress conditions, the effect of contact between crack flanks is highly noticeable, as highlighted in Fig. 10 (b). In fact, for both specimens, the FCG rate is significantly higher (approximately twice) when the contact between the flanks is neglected in the simulation. Note that neglecting the contact between the crack flanks does not affect the influence of the drilled holes on the FCG rate. In fact, without contact the effect of the holes is even more pronounced. Therefore, the crack closure phenomenon is able to explain different issues of FCG, but not the effect of crack flank holes.

The evolution of the crack closure level during the crack propagation, predicted under plane stress state for different values of diameter, is shown in Fig. 11. In the present study, the crack opening level was evaluated through the contact status of the first node behind the crack tip, defined by:

$$U^* = \frac{F_{open} - F_{min}}{F_{max} - F_{min}} \tag{3}$$

where F_{open} is the crack opening load. This parameter quantifies the fraction of the load cycle for which the crack remains closed. As mentioned before, the dashed vertical lines represent the border of each hole, while all of them are centred at a crack length corresponding to 16 mm.

The specimen with the biggest holes ($D = 1.5$ mm) leads to a lower value of crack closure. However, this value increases as the crack crosses the hole diameter. The specimens with the small holes ($D = 1.0$ mm and $D = 0.5$ mm) show a different behaviour. Accordingly, the crack closure increases as the crack approaches the centre of the holes and then decreases as it travels further away from this point. The crack closure is higher in the specimen without drilled holes, as shown in Fig. 11. Therefore, the effect of the crack flank holes on the FGC rate (see Fig. 7) is not directly related to the crack closure since it is always higher for the specimen without holes.

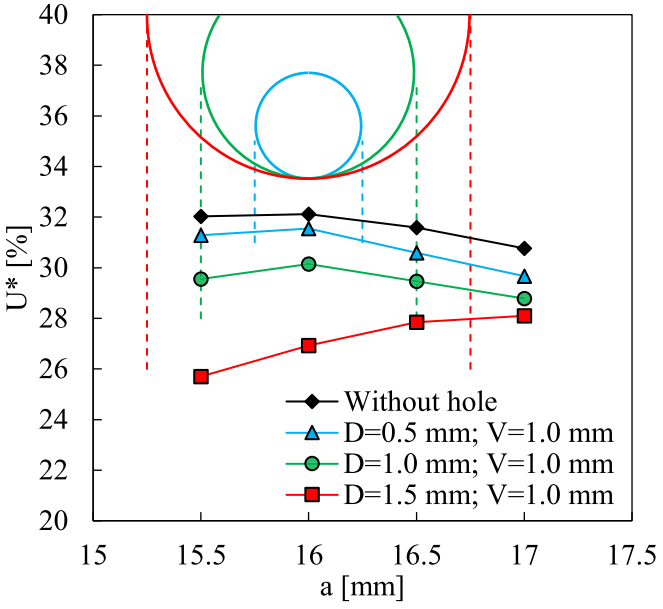

Fig. 11. Evolution of the crack closure level (U^*) during the crack propagation predicted under plane stress for different values of holes diameter ($V = 1.0$ mm).

4. Validation with experimental results

The validation of the adopted finite element model was carried out by using the experimental analysis of a CT specimen with two pairs of drilled holes, allowing to evaluate the accuracy of the numerical results. Fig. 12 presents the geometry and the main dimension of the specimen, presenting 2 mm of nominal thickness, 1 mm of the notch gap and 60° of notch tip angle. Using the nomenclature of Fig. 1, the first pair of drilled holes is defined by $D_1 = 2.0$ mm and $V_1 = 2.0$ mm, corresponding to a crack length of $a_1 = 14$ mm, while the second pair of drilled holes is defined by $D_2 = 2.0$ mm and $V_2 = 1.0$ mm, corresponding to a crack length of $a_2 = 25$ mm. Thus, the distance between the two pairs of holes is 11 mm, allowing to study each one independently.

The fatigue crack growth tests were performed according to ASTM E647 standard [20], at room temperature using a 10 kN capacity Instron EletroPuls E10000 machine (Instron, Norwood, MA, USA), under loading control and a stress ratio of R = 0.1, at a loading frequency of 10 Hz. The crack length was measured by optical method using a travelling

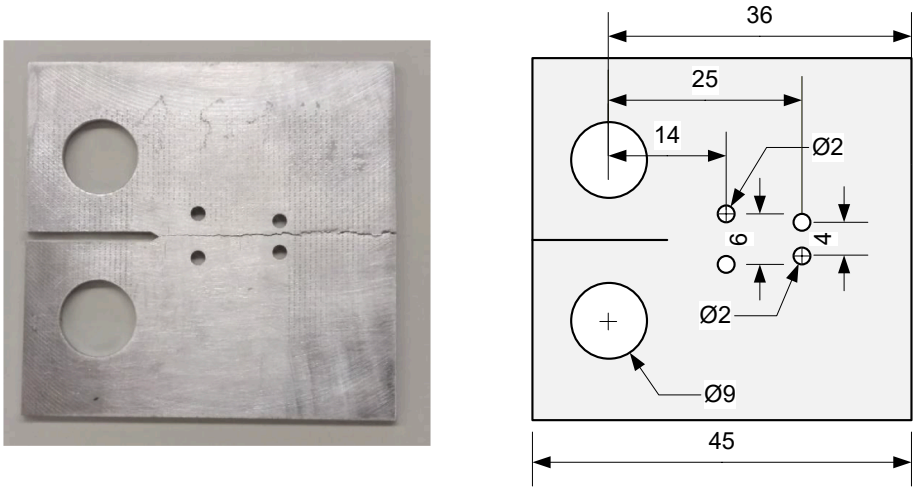

Fig. 12. CT specimen used in the validation of the numerical model: (a) specimen used in the experimental test; (b) geometry and main dimensions of the specimen.

microscope (45 ×) in increments of 0.2 mm. The tests were conducted under constant load amplitude, i.e., under increasing ΔK. Nevertheless, different values of load range were considered for each pair of drilled holes, to avoid different orders of magnitude in the values of the FCG rate. The maximum and minimum values of load applied in the experimental test are listed in Table 4 for each pair of holes. They were obtained taking into account the results of Section 3, i.e. the load range was determined to obtain a stress intensity factor range value (without holes) similar to the one obtained previously in the parametric study. When the crack tip crossed the line connecting the centres of the first holes ($a = 14$ mm) the stress intensity factor range was $\Delta K = 13.1$ MPa.m$^{0.5}$, while when the crack tip crossed the line connecting the centres of the second holes ($a = 25$ mm) the stress intensity factor range was $\Delta K = 16.2$ MPa.m$^{0.5}$.

The specimens used in this experimental analysis were built in AA2050-T8 aluminium alloy, obtained along the S-T orientation. Regarding the mechanical behaviour of this aluminium alloy, purely kinematic hardening was considered to describe the plastic behaviour in the numerical model. Thus, the Lemaitre-Chaboche non-linear kinematic hardening law was adopted, using the parameters listed in Table 5, which were obtained by fitting the mid-life cyclic stress–strain hysteresis loops evaluated using low-cycle fatigue tests [37]. The critical value of plastic strain involved in the node release approach was obtained using the calibration procedure previously described, obtaining $\varepsilon_p^c = 110$ %.

Due to the small thickness of the CT specimens used in the experimental approach, the numerical analysis was performed under plane stress conditions. Besides, the thickness of the specimens used in the numerical model was 0.1 mm, allowing to use a single layer of finite elements throughout the thickness. Accordingly, the load range used in the numerical model was reduced by a factor of 20. In order to reduce the computational cost, two different simulations were performed independently, one for each pair of holes. Accordingly, two different finite element meshes were created, using linear hexahedral finite elements. In both cases, the length of the crack path crossing the drilled holes was 6 mm, where the mesh was refined to achieve an element size of 8 μm.

Table 4
Maximum and minimum values of load applied in the experimental test for each pair of holes.

	a_0 [mm]	F_{min} [N]	F_{max} [N]
First pair of holes ($D = 2$ mm; $V = 2$ mm)	10	88.89	888.9
First pair of holes ($D = 2$ mm; $V = 1$ mm)	19	47.72	472.2

Table 5
Mechanical properties for the 2050-T8 aluminium alloy [37].

Young Modulus [GPa]	Poisson's Coefficient	Lemaitre-Chaboche model		
		Y_0 [MPa]	X_{Sat} [MPa]	C_X
70	0.33	316.87	188.64	416.88

Fig. 13 presents the FCG rate evolution when the crack crosses the first pair of holes, compared with the situation of the specimen without holes. The dashed vertical lines represent the left and right limits of the holes. The numerical predictions (Fig. 13 (b)) are in good agreement with the experimental measurements (Fig. 13 (a)). Note that the severe decrease of the predicted FCG rate at the beginning is due to the formation of the plastic wake. The inclusion of the crack flank holes ($D = 2.0$ mm and $V = 2.0$ mm) leads to an increase of the FCG rate while the holes are located ahead of the crack tip. On the other hand, when the holes are located behind the crack tip the effect of the drilled holes on the FCG rate is negligible. Thus, the inclusion of the flank holes is globally detrimental to fatigue life.

The evolution of the FCG rate when the crack crosses the second pair of holes is presented in Fig. 14 and compared with the results obtained for the specimen without holes. The dimensions of the specimens used in the experimental test are slightly different from the ones used in the numerical model due to some difficulties in the specimen preparation. The only difference is in the location of the second pair of drilled holes, which are located at 24.5 mm in the physical specimen. Thus, the location of this second pair of holes, denoted by the dashed vertical lines, is slightly different comparing the experimental (Fig. 14 (a)) and numerical results (Fig. 14 (b)). The effect of the crack flank holes on the FCG rate is stronger in the second pair of holes in comparison with the first pair since the distance between the symmetrically drilled holes is shortened (see Fig. 12 (b)). Considering the crack tip located behind the drilled holes, the FCG rate measured in the specimen with crack flank holes ($D = 2.0$ mm and $V = 1.0$ mm) is higher in comparison with the specimen without holes. This difference in the FCG rate increases as the crack tip approaches the left limit of the holes, where the FCG rate for the specimen with drilled holes is at least twice the value evaluated in the specimen without holes. After the crack tip crosses the holes, the effect of the drilled holes on the FCG rate vanishes in the experimental measurements whiles becoming negligible in the numerical predictions. Indeed, the numerical model predicts a slight reduction of the FCG rate in comparison with the situation without drilled holes. Nonetheless, the

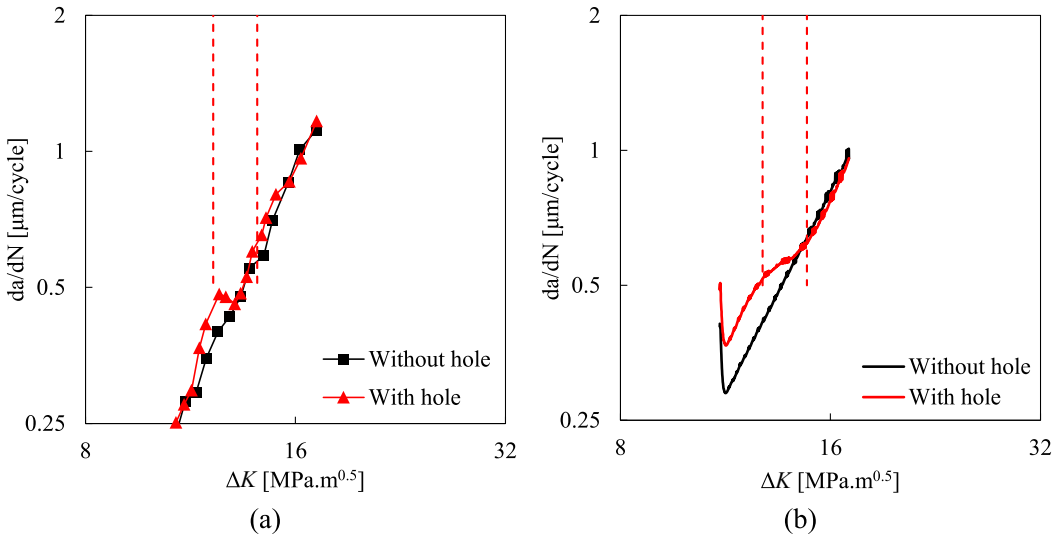

Fig. 13. Effect of the first pair of holes on the FCG rate: (a) experimental measurement; (b) numerical prediction.

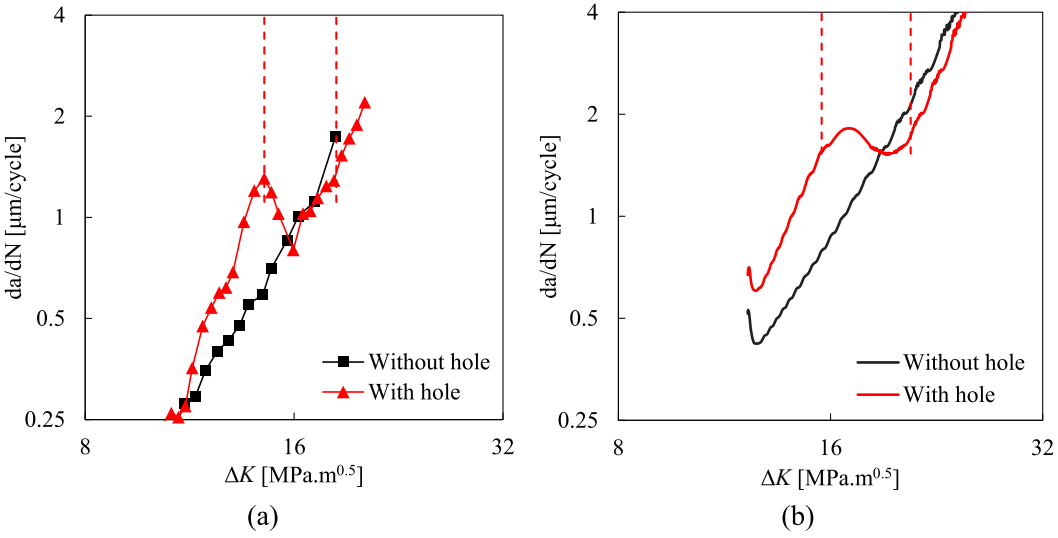

Fig. 14. Effect of the second pair of holes on the FCG rate: (a) experimental measurement; (b) numerical prediction.

inclusion of the crack flank holes has a detrimental effect on the fatigue life. Globally, the numerical predictions are in good agreement with the experimental measurements, as highlighted in Fig. 14. Therefore, the adopted numerical approach, which is based on the cumulative plastic deformation at the crack tip, is able to predict the FCG rate and can be used to study other geometrical or loading effects. This also indicates that cyclic plastic deformation is the main damage mechanism responsible for FCG.

5. Conclusions

The effect of drilling two symmetric holes along the crack flanks on the fatigue crack growth rate was evaluated numerically in the present study. The parametric study was carried out for the 2024-T351 aluminium alloy using CT specimens, considering different values for the diameter of holes and the distance between them. The finite element model was validated by comparing the numerical predictions with experimental measurements, using a CT specimen made of 2050-T8 aluminium alloy with two pairs of drilled holes along the crack flanks. The main conclusions are:

- The fatigue crack growth rate increases when the drilled holes are located ahead of the crack tip and decreases when holes are located behind the crack tip. Overall, the inclusion of the crack flank holes has a detrimental effect on the fatigue life.
- Increasing the diameter of the holes leads to an increase of the effect on the FCG rate.
- Decreasing the distance between the holes (closer to the crack path) leads to an increase of the effect on the FCG rate.
- The effect of the holes is not due to the crack closure phenomenon. Anyway, the crack closure level in the specimen without holes is about 32 %. Increasing the diameter of the holes leads to a global decrease of the crack closure level. Neglecting the contact between the crack flanks in the numerical model is admissible under plane strain conditions, but it leads to a significant increase of the FCG rate under plane stress conditions.
- The effect of the holes is linked to a geometrical effect on crack tip strain. Comparing with the specimen without holes, the presence of the drilled holes leads to an increase (decrease) of the plastic zone size when the crack tip is located immediately behind (ahead) of the holes.

- The numerical predictions are in good agreement with the experimental measurements of the FCG rate, highlighting the accuracy of the finite element model. Besides, this indicates that the cumulative plastic strain is an adequate crack driving force and that cyclic plastic deformation is expected to be the main damage mechanism responsible for fatigue crack growth.

Declaration of Competing Interest

The authors declare that they have no known competing financial interests or personal relationships that could have appeared to influence the work reported in this paper.

Data availability

Data will be made available on request.

Acknowledgements

The authors gratefully acknowledge the financial support through the Portuguese Foundation of Science and Technology (FCT) under the projects UIDB/00285/2020 and LA/P/0112/2020. Edmundo Sérgio is also grateful to the FCT for the PhD grant with reference 2022.11438.BD.

References

[1] Elber W. Fatigue crack closure under cyclic tension. Eng Fract Mech 1970;2:37–45.
[2] Borrego LP, Ferreira JM, Costa JM. Fatigue crack growth and crack closure in an AlMgSi alloy. Fatigue Fract Eng Mater Struct 2001;24:255–65.
[3] Borges MF, Neto DM, Antunes FV. Revisiting classical issues of fatigue crack growth using a non-linear approach. Materials 2020;13:5544.
[4] Borrego LP, Ferreira JAM, Pinho da Cruz JM, Costa JM. Evaluation of overload effects on fatigue crack growth and closure. Eng Fract Mech 2003;70:1379–97.
[5] Neto DM, Borges MF, Antunes FV, Sunder R. Numerical analysis of fatigue crack growth under SuperBlock2020 loading sequence. Eng Fracture Mech 2022;260(1):108178.
[6] Neto DM, Borges MF, Sérgio ER, Antunes FV. Effect of residual stresses on fatigue crack growth: a numerical study based on cumulative plastic strain at the crack tip. Mater Mater 2022;15(6):2156.
[7] Costa JDM, Ferreira JAM. Effect of stress ratio and specimen thickness on fatigue crack growth of CK45 steel. Theor Appl Fract Mech 1998;30:65–73.
[8] Borges MF, Caldas M, Antunes FV, Branco R. Pedro Prates, Fatigue crack growth from notches: a numerical analysis. Appl Sci Appl Sci 2020;10:4174.
[9] Tong J. T-stress and its implications for crack growth. Eng Fract Mech 2002;69:1325–37.
[10] Atatollahi MR, Razavi SMJ, Chaman HR. A numerical study on the effect of symmetric crack flank holes on fatigue life extension of a SENT specimen. Fatigue Fract Eng Mater Struct 2014;37:1153–64.
[11] Shin CS, Wang CM, Song PS. Fatigue damage repair: a comparison of some possible methods. Int J Fatigue 1996;18:535–46.
[12] Chen H, Chen W, Li T, Ure J. Effect of circular holes on the ratchet limit and crack tip plastic strain range in a centre cracked plate. Eng Fract Mech 2011;78:2310–24.
[13] Aviation maintenance technician handbook – airframe, vol. 1, Chapter 04. U.S. Department of transportation, Federal aviation administration, Flight standards service; 2012.
[14] Miki C. Retrofitting engineering for fatigue damaged steel structures. International institute of welding, Doc. IIW-XIII-2284r1-09; 2010.
[15] Repair of bridge structural steel elements manual (Release 1.0). Technical standards branch. Alberta transportation; 2004.
[16] Song PS, Shieh YL. Stop drilling procedure for fatigue life improvement. Int J Fatigue 2004;26:1333–9.
[17] Ghfiri R, Amrouche A, Imad A, Mesmacque G. Fatigue life estimation after crack repair in 6005 AT-6 aluminum alloy using the cold expansion hole technique. Fatigue Fract Eng Mater Struct 2000;23:911–6.
[18] Makabe C, Murdani A, Kuniyoshi K, Irei Y, Saimoto A. Crack-growth arrest by redirecting crack growth by drilling stop holes and inserting pins into them. Eng Fail Anal 2009;16:475–83.
[19] Razavi SMJ, Ayatollahi MR, Sommitsch C, Moser C. Retardation of fatigue crack growth in high strength steel S690 using a modified stop-hole technique. Eng Fract Mech 2017;169:226–37.
[20] Feng M, Ding F, Jiang Y. A study of crack growth retardation due to artificially induced crack surface contact. Int J Fatigue 2005;27:1319–27.
[21] Khaburskyi Y, Slobodyan Z, Hredil M, Nykyforchyn H. Effective method for fatigue crack arrest in structural steels based on artificial creation of crack closure effect. Int J Fatigue 2019;127:217–21.
[22] Ayatollahi MR, Hashemi R. Mixed mode fracture in an inclined center crack repaired by composite patching. Compos Struct 2007;81:264–73.
[23] Chen BD, Griffiths JR, Lam YC. The effects of simultaneous overload and spot heating on crack growth retardation in fatigue. Eng Fract Mech 1993;44(4):567–72.
[24] Lim WK, Yoo JS, Choi SY. The effects of concurrent cold-expansion and ring-indentation on the growth of fatigue cracks emanating from circular holes. Eng Fract Mech 1998;59(5):643–53.
[25] Ruzek K, Pavlas J, Doubrava R. Application of indentation as a retardation mechanism for fatigue crack growth. Int J Fatigue 2012;37:92–9.
[26] Chahardehi A, Brennan FP, Steuwer. The effect of residual stresses arising from laser shock peening on fatigue crack growth. Eng Fract Mech 2010;77(11):2033–9.
[27] Huang S, Zhou JZ, Sheng J, Lu JZ, Sun GF, Meng XK, et al. Effects of laser energy on fatigue crack growth properties of 6061–T6 aluminum alloy subjected to multiple laser peening. Eng Fract Mech 2013;99:87–100.
[28] Bagherifard S, Guagliano M. Fatigue behavior of a low-alloy steel with nanostructured surface obtained by severe shot peening. Eng Fract Mech 2012;81:56–68.
[29] Liu TJC. Finite element modeling of melting crack tip under thermo-electric Joule heating. Eng Fract Mech 2011;78(4):666–84.
[30] Borges MF, Neto DM, Antunes FV. Numerical simulation of fatigue crack growth based on accumulated plastic strain. Theor Appl Fract Mech 2020;108:102676.
[31] Borges MF, Antunes FV, Moreno B, Prates P, Camas D, Neto DM. Fatigue crack propagation analysis in 2024–T351 aluminium alloy using nonlinear parameters. Int J Fatigue 2021;153:106478.
[32] Neto DM, Borges MF, Antunes FV. Mechanisms of fatigue crack growth in single overloads. Theor Appl Fract Mech 2021;114:103024.
[33] Neto DM, Sérgio ER, Borges MF, Borrego LP, Antunes FV. Effect of load blocks on fatigue crack growth. Int J Fatigue 2022;162:107001.
[34] Menezes LF, Teodosiu C. Three-dimensional numerical simulation of the deep-drawing process using solid elements. J Mater Process Technol 2000;97:100–6.
[35] Swift HW. Plastic instability under plane stress. J Mech Phys Solids 1952;1:1–18.
[36] Frederick CO, Armstrong PJ. A mathematical representation of the multiaxial Bauschinger effect. Mater High Temp 2007;24:1–26.
[37] Jesus JS, Antunes FV, Prates P, Branco R, Antunes PV, Borrego LP, et al. Influence of specimen orientation on fatigue crack growth in 7050–T7451 and 2050–T8 aluminium alloys. Int J Fatigue 2022;164:107136.